

## EVOLUTION OF YOUNG NEUTRON STAR ENVELOPES

PHILIP CHANG

Department of Physics, Broida Hall, University of California, Santa Barbara, CA 93106; pchang@physics.ucsb.edu

AND

LARS BILDSTEN

Kavli Institute for Theoretical Physics and Department of Physics, Kohn Hall, University of California, Santa Barbara, CA  
93106; bildsten@kitp.ucsb.edu

Draft version October 31, 2018

## ABSTRACT

We extend our initial study of diffusive nuclear burning (DNB) for neutron stars (NSs) with Hydrogen atmospheres and an underlying layer of proton capturing nuclei. Our initial study showed that DNB can alter the photospheric abundance of Hydrogen on surprisingly short timescales ( $10^{2-4}$  yrs). Significant composition evolution impacts the radiated thermal spectrum from the NS as well as its overall cooling rate. In this paper, we consider the case when the rate limiting step for the H consumption is diffusion to the burning layer, rather than the local nuclear timescale. This is relevant for NSs with surface temperatures in excess of  $10^6$  K, such as young ( $< 10^5$  yr) radio pulsars and accreting NSs in quiescence. When downward diffusion is the limiting rate in DNB, the rate of H consumption is suppressed by 1-2 orders of magnitude compared to a DNB estimate that assumes diffusive equilibrium. In order to apply our ongoing study to young neutron stars, we also include the important effects of strong magnetic fields ( $B \sim 10^{12}$  G). In this initial study of magnetic modifications to DNB, we find that the H burning time is lengthened by 2-3 orders of magnitude for a  $10^{12}$  G field. However, even for NSs with dipole field strengths of  $10^{12}$  G, we find that all of the H can be burned before the pulsar reaches an age of  $\sim 10^5$  yr, thus potentially revealing the underlying proton-capturing elements. Finally, we conclude by providing an overview of what can be learned about fallback and pulsar winds from measuring the surface composition of a young NS.

*Subject headings:* diffusion – magnetic fields – nuclear reactions, nucleosynthesis, abundances – pulsars: general – stars: abundances, interiors – stars: neutron

## 1. INTRODUCTION

The surface compositions of young NSs are now regularly probed by Chandra and XMM-Newton observations (see Pavlov, Zavlin & Sanwal 2002a for a review; also see Sanwal et al. 2002; Mereghetti et al. 2002; Bignami et al. 2003). Since the amount of matter in the photosphere is small ( $\sim 10^{-20} M_\odot$ ), there is no reliable way to predict the composition of these outer layers from supernova theory. Fall-back during the supernovae event (or later) could provide a large range of possible elements (Woosley & Weaver 1995), ranging from pure H (due to spallation of heavier elements; Bildsten, Salpeter & Wasserman 1992), mid-weight material (due to a “soft-landing” of outer shells falling back), or iron (if no fallback occurred).

The current X-ray observations of young radio pulsars suggest that those younger than  $\sim 10^{4-5}$  yrs possess magnetic H or He atmospheres (Pavlov, Zavlin & Sanwal 2002a), whereas pulsars older than  $\sim 10^{4-5}$  yrs possess heavier element atmospheres (see Pavlov et al. 2002b and references therein; also see Kaminker, Yakovlev & Gnedin 2002). This suggests a possible evolution of H or He to more blackbody-like elements on a timescale of  $10^{4-5}$  yrs, and motivated our work (Chang & Bildsten 2003; hereafter CB03) on a mechanism of nuclear evolution called diffusive nuclear burning (DNB) (first mentioned by Chiu & Salpeter 1964 and later calculated by Rosen 1968) that provides for a surprisingly rapid depletion of H.

The physics of DNB is very simple. At the photosphere, the local temperature ( $T_e \sim 10^6$  K) and density ( $\rho \sim 1 \text{ g cm}^{-3}$ ) are far too low to drive nuclear burning. However, 1 meter underneath the photosphere, the density and temperature are much higher ( $\rho \sim 10^{5-6} \text{ g cm}^{-3}$ ,  $T \sim 10^8$  K) so any surface H that dif-

fuses down to this region will be rapidly captured onto a heavier nucleus. For example, for H capture onto Carbon, the  $^{13}\text{C}$  produced in this reaction (following the  $\beta$  decay of  $^{13}\text{N}$ ) sinks into the NS. This H depletion at depth then drives a H current from the surface that, over time, can completely deplete the H at the photosphere. The surprising realization is that the consumption of H is set by burning which occurs in the exponentially suppressed diffusive tail, and can easily consume all of the H on a NS in timescales of  $\sim 10^5$  years.

In CB03, we found that at the characteristic depth,  $y_{\text{burn}}$  (i.e. the burning layer), where the H is rapidly consumed, there was adequate time for diffusive equilibrium to be established for  $T_c < 5 \times 10^7$  K for H on C. Hence at these low  $T_c$ 's (and therefore low  $T_e$ 's), the rate limiting step is nuclear processes rather than diffusion. However, at higher  $T_c$ 's typical of young NSs, the nuclear timescale,  $\tau_{\text{nuc}}$ , rapidly drops below the diffusion timescale,  $\tau_{\text{diff}}$ , so that diffusive equilibrium no longer holds and downward diffusion to the burning layer is the rate limiting step. The simple estimate for this transition to diffusion-limited DNB is when  $\tau_{\text{nuc}} \sim \tau_{\text{diff}}$ , where  $\tau_{\text{diff}} = h^2 / D$  is the time for H to diffuse an ion scale height,  $h$ . We find that incorporating the effects of diffusion into DNB decreases H consumption by 1-2 orders of magnitude or greater at high  $T_c$  compared to a naive calculation assuming diffusive equilibrium. In addition, the dependence of the rate of H consumption with  $T_c$  changes when diffusion is the rate limiting step. Because of the size of the effects of diffusion at high  $T_c$  on DNB, we only use an approximate treatment of diffusion in our estimates of DNB rates.

In addition, we also include the modification of the thermal profile due to the opacity changes induced by such high  $B$  fields

(Ventura & Potekhin 2001; Potekhin & Yakovlev 2001), since nearly all young neutron stars are also strongly magnetic ( $B \sim 10^{12}$  G). We find that strong magnetic fields alter the burning rate due to the modification of the thermal profile by 2-3 orders of magnitude.

Applying our estimates to young NSs, we find that the age after which DNB is no longer active is roughly  $10^{5-6}$  years for standard cooling (and much sooner for rapid cooling). Prior to the cessation of DNB, H is always depleted on a timescale shorter than the present age. Following Michel (1975), we show that pulsar wind excavation of the NS surface is potentially a powerful mechanism for composition evolution. In particular, the pulsar wind can excavate to depths that exceed the maximum thickness allowed for a H or He layer due to thermonuclear constraints.

This paper is structured as follows. In § 2 we discuss the basic equations and their modification in the limit where diffusion is the rate limiting step. We discuss the effects of the magnetic field on the envelope's thermal structure and DNB in § 3, which then allows us to apply our work to young neutron stars in § 4. We also speculate on the possible excavation of material of NSs due to ion loss in a pulsar wind. We conclude in § 5 by summarizing our results and providing our views on what can be learned from measurements of young NS surface composition.

## 2. DIFFUSION LIMITED DNB

We only consider the top  $10^4$  cm of the envelope, where the density is  $< 10^{10}$  g cm $^{-3}$ . The thickness of this layer is  $\ll R$ , so we assume a plane parallel atmosphere with constant downward gravitational acceleration,  $g$ . Consider an envelope consisting of protons, electrons and ions that are coupled to each other and obey charge neutrality ( $n_e = \sum_i Z_i n_i$ ). The equations of hydrostatic balance are,

$$\frac{dP_p}{dr} = -n_p [m_p g - eE + r_{ep} n_e (v_p - v_e) + r_{ip} n_i Z_i^2 (v_p - v_i)], \quad (1a)$$

$$\frac{dP_i}{dr} = -n_i [A_i m_p g - Z_i eE + r_{ep} n_e Z_i^2 (v_i - v_e) + r_{ip} n_p Z_i^2 (v_i - v_p)], \quad (1b)$$

$$\frac{dP_e}{dr} = -n_e [m_e g + eE + r_{ep} n_i Z_i^2 (v_e - v_i) + r_{ep} n_p (v_e - v_p)], \quad (1c)$$

where  $P_i$ ,  $n_i$ ,  $A_i$ ,  $Z_i$ ,  $v_i \equiv J_i/n_i$  are the pressure, number density, atomic number, charge and relative velocity of the  $i$ 'th ion species in Eulerian coordinates and  $E$  is the upward pointing electric field. General relativistic effects have been ignored. For simplicity, we presume the ions obey an ideal gas equation of state, neglecting effects such as plasma nonideality. We also ignore thermal diffusion effects, which are expected to play only a minor role in determining the structure of the NS envelope as the temperature scale height is larger than the ion scale height. In addition the thermal diffusion coefficient is small and hence thermal diffusion effects are expected to be minor compared to ordinary diffusion or gravitational settling in dense plasmas (Paquette et al. 1986 in the case of trace fully-ionized C in fully-ionized He). Plasma non-ideality effects are more significant especially for determining the structure of an envelope with two or more species with the same A/Z (i.e. He, C, N, O) and is an interesting question that needs to be addressed in the future. In the dense regions of the plasma, plasma non-ideality effects are expected to come in as  $P_{\text{Coulomb}}/P$ , where  $P_{\text{Coulomb}}$  would be the Coulomb pressure and  $P$  is the local pressure, which could be large (as large as 20%) in the region of interest. Plasma non-ideality effects could be particularly significant in the case of

highly magnetized plasmas ( $B > 10^{11}$  G) as the Fermi pressure is decreased by the presence of a quantizing magnetic field (Lai 2001). Hence our model is very simplified, but captures the essential physics of this problem. All vectorial quantities are positive radially. The coupling coefficient,  $r_{jl}$ , is due to scattering of species  $j$  by species  $l$ . In CB03, we consider the case where these velocities are small, so that these drag terms could be neglected. However, this is not the case here.

We consider the case where the protons are a drifting trace and the ions and electrons are a fixed background so  $v_e \approx v_i \approx 0$  and  $n_e \approx Z_i n_i \gg n_p$ . Equations (1) simplify to

$$\frac{dP_p}{dr} = -n_p (m_p g - eE + r_{ip} n_i Z_i^2 v_p), \quad (2a)$$

$$\frac{dP_i}{dr} = -n_i (A_i m_p g - Z_i eE), \quad (2b)$$

$$\frac{dP_e}{dr} = -n_e (m_e g + eE). \quad (2c)$$

We have dropped the drag terms in the ion and electron hydrostatic balance equations since the drag force exerted on them by the protons is  $\ll m_p g$ . The drag term in the proton hydrostatic balance equation is only relevant in the presence of a nontrivial proton current,  $J_p \equiv n_p v_p$ . The drag coefficient is simply related to the diffusion coefficient,  $\mathcal{D}$ , by taking the definition of the current,

$$J_p = -\mathcal{D} \frac{dn_p}{dr} + n_p w_p = n_p v_p, \quad (3)$$

where  $w_p$  is the proton drift velocity, and relating it to our equations of hydrostatic balance. To begin let us presume that no current exists ( $J_p = 0$ ) so that equation (3) becomes  $d \ln n_p / dr = w_p / \mathcal{D}$ . For an isothermal atmosphere the proton hydrostatic balance equation is

$$\frac{d \ln n_p}{dr} = \frac{-m_p g + eE}{k_B T}, \quad (4)$$

which when equated to that from the diffusion equation gives  $w_p / \mathcal{D} = (-m_p g + eE) / k_B T$ . For  $J_p \neq 0$ , the proton equation of hydrostatic balance is

$$\frac{d \ln n_p}{dr} = \frac{-m_p g + eE - r_{ip} n_i Z_i^2 v_p}{k_B T}, \quad (5)$$

whereas the diffusion equation becomes

$$\frac{d \ln n_p}{dr} = \frac{w_p - v_p}{\mathcal{D}}. \quad (6)$$

Taking our earlier expression for  $w_p$  and equating equations (5) and (6) yields the relation,

$$r_{ip} = \frac{k_B T}{n_i Z_i^2 \mathcal{D}}, \quad (7)$$

between the drag and diffusion coefficients.

In the limit of ideal gases, when Coulomb corrections to the ion equation of state are small ( $\Gamma \equiv Z^2 e^2 / (a k_B T) < 1$ , where  $a$  is the interionic spacing), we parameterized  $\mathcal{D}$  using the results of Chapman & Cowling (1952) (also see Alcock & Illarionov 1980). In the liquid regime ( $1 < \Gamma < 175$ ), where most of the burning occurs, we begin with the fit of Hansen, McDonald & Pollock (1975) of the dimensionless self diffusion coefficient,  $\mathcal{D}^* = \mathcal{D}_s / (\omega_p a^2) 2.95 \Gamma^{-4/3}$ , where  $\omega_p$  is the plasma frequency and  $a$  is the mean ion separation. We compute the interspecies diffusion coefficient from the self-diffusion coefficient in the same manner as Brown, Bildsten & Chang (2002). We assume the Stokes-Einstein relation,  $\mathcal{D}_s / k_B T = (4\pi a_1 \eta)^{-1}$ , where  $a_1$  is

the charge neutral sphere of the background species and  $\eta$  is the viscosity. The diffusion coefficient for a trace in a background is  $\mathcal{D}/k_B T = (4\pi a_2 \eta)^{-1}$ , where  $a_2$  is the charge neutral sphere around the trace. Hence we find  $\mathcal{D} = \mathcal{D}_s a_1/a_2$ , which gives

$$\mathcal{D} \approx 10^{-3} \frac{A_1^{0.1} T_6^{1.3}}{Z_1^{1.3} Z_2^{0.3} \rho_5^{0.6}} \text{ cm}^2 \text{ sec}^{-1}, \quad (8)$$

where 1 and 2 are the background and trace ion respectively,  $T_6 = T/10^6 \text{ K}$  and  $\rho_5 = \rho/10^5 \text{ g cm}^{-3}$ . The burning layer is usually in the liquid region unless the effective temperature is extremely high or low. The self-diffusion coefficient fitted by Hansen et al. (1975) is off by 50% at  $\Gamma \approx 1$ , compared to the more complete calculation of Paquette et al. (1986), but is accurate to within a few percent for  $\Gamma > 10$ . The work of Paquette et al. (1986) presents a more consistent way of bridging the transition from the dilute approximate of Chapman & Cowling and the strong coupling results of Hansen et al. (1975), but for our estimates equation (8) is adequate in the liquid regime. At extremely low  $T_e$ 's, the burning layer crystallizes ( $\Gamma > 175$  for a one-component plasma; Potekhin & Chabrier 2000) and halts diffusion.

The thermal structure is determined by the heat diffusion equation for a constant flux,

$$\frac{dT}{dr} = -\frac{3\kappa\rho}{16T^3} T_e^4, \quad (9)$$

where  $\kappa$  is the opacity. The radiative opacity is determined mostly by free-free absorption, where the Gaunt factor,  $g_{\text{ff}}$ , is fitted by Schatz et al. (1999). We use the conductive opacities given by Baiko et al. (1998) with analytic formulae given by Potekhin et al. (1999a). For NSs with low surface magnetic fields ( $B < 10^9 \text{ G}$ ), we use the Paczynski (1983) electron equation of state (which is accurate to within 5% for ideal electron plasmas).

The continuity equation for the protons is

$$\frac{\partial n_p}{\partial t} + \frac{dJ_p}{dr} = -\frac{n_p}{\tau_{p,\text{nuc}}}, \quad (10)$$

where  $\tau_{p,\text{nuc}}$  is the local proton lifetime against nuclear capture. As we have argued in CB03, the timescale for changing the local number density is the timescale for changing the Hydrogen column, which is much longer than the local nuclear timescale. Hence, we take a steady state approximation ( $\partial n_p/\partial t = 0$ ), which provides the current induced by DNB. We combine equations (3), (5) and (10) to obtain

$$\frac{d^2 n_p}{dr^2} + \frac{dn_p}{dr} l_p^{-1} - n_p \frac{r_{ip} n_i Z_i^2}{k_B T \tau_{p,\text{nuc}}} = 0, \quad (11)$$

where  $l_p = k_B T / (eE - m_p g)$  is the proton scale height.

Another way to derive equation (11) is to combine the proton continuity equation (eq. [10]) with the definition of the current (eq.[3]) to obtain

$$-\frac{d^2 n_p}{dr^2} + \frac{w_p}{\mathcal{D}} \frac{dn_p}{dr} + \frac{n_p}{\mathcal{D} \tau_{p,\text{nuc}}} = 0, \quad (12)$$

where for the purposes of this discussion we presume  $\mathcal{D}$  and  $w_p$  are constants. Our full analysis includes the position dependence of  $\mathcal{D}$  and  $w_p$  in equation (12). However, we will argue that only two terms really matter in the final analysis. Taken with equation (7), we see that equation (12) is equivalent to equation (11).

Care must be taken when solving equation (12) since  $\tau_{p,\text{nuc}}$  has a powerful temperature dependence. We write  $n_p = \mathcal{F}_p n_{p,0}$ ,

in terms of a scaling factor  $\mathcal{F}_p$  and  $n_{p,0}$ , the solution in diffusive equilibrium. After dividing by  $n_{p,0}$ , equation (12) becomes,

$$\frac{\mathcal{F}_p}{n_{p,0}} \left( -\mathcal{D} \frac{d^2 n_{p,0}}{dr^2} + \frac{dn_{p,0}}{dr} w_p \right) + \frac{d\mathcal{F}_p}{dr} \left( -\mathcal{D} \frac{d \ln n_{p,0}}{dr} + w_p \right) - \mathcal{D} \frac{d^2 \mathcal{F}_p}{dr^2} - \mathcal{D} \frac{d\mathcal{F}_p}{dr} \frac{d \ln n_{p,0}}{dr} = -\frac{\mathcal{F}_p}{\tau_{p,\text{nuc}}}. \quad (13)$$

The first term in parentheses is the homogeneous diffusion equation and hence it is zero, while the second term,  $-d \ln n_{p,0}/dr + l_p^{-1}$ , is the ion equation of hydrostatic balance and is solved by  $n_{p,0}$ , making this term zero as well. Thus the full diffusion equation reduces to

$$\frac{d^2 \mathcal{F}_p}{dr^2} + \frac{d\mathcal{F}_p}{dr} \frac{d \ln n_{p,0}}{dr} = \frac{\mathcal{F}_p}{\mathcal{D} \tau_{p,\text{nuc}}}, \quad (14)$$

which we solve with the boundary conditions  $\mathcal{F}_p \approx 1$  and  $d\mathcal{F}_p/dr \approx 0$  far above the burning layer. Since  $\tau_{p,\text{nuc}}$  is a nuclear timescale, which falls very rapidly as we move into the deeper, hotter regions of the envelope, the nuclear scale height,  $l_{\text{nuc}}^2 \equiv \mathcal{D} \tau_{p,\text{nuc}}$ , rapidly decreases into the envelope. Hence the second term in equation (14) rapidly becomes insignificant as the proton scale height,  $l_p = (d \ln n_{p,0}/dr)^{-1}$  becomes  $\gg l_{\text{nuc}}$  at the burning layer. Thus for all practical purposes, the second term could be dropped and we would have a diffusion equation for  $\mathcal{F}_p$  with a nuclear driven source. Therefore,  $\mathcal{F}_p$  defines the departure from diffusive equilibrium at a given depth as a result of nuclear burning. If we include the position dependence of  $\mathcal{D}$  and  $w_p$ , this would not change our result significantly since inclusion of those terms would introduce additional terms with  $l_p$  and the thermal scale height,  $l_T = (d \ln T/dr)^{-1}$ , both of which are  $\gg l_{\text{nuc}}$  at the burning layer. The total diffusive current is given by

$$\zeta_H = \frac{y_H}{\tau_{\text{col}}} = \int \frac{\mathcal{F}_p n_{p,0}}{\tau_{p,\text{nuc}}} dr = \int \frac{\mathcal{F}_p n_{p,0}}{\tau_{p,\text{nuc}}} \frac{y}{\rho} d \ln y, \quad (15)$$

where  $y = P/g$  is the total column density,  $\rho$  is the local density and  $\tau_{\text{col}}$  is the H column lifetime.

Figure 1 shows the thermal and compositional structure of the envelope (eq. [2a], [9] and [14]) and the total burning rate,  $\zeta_H$ . We also solve the model assuming full diffusive equilibrium (CB03). The burning cuts off the H number concentration at large columns. The exponential increase in burning rates modifies the solution for the total diffusive current by a factor of two compared to the case of full diffusive equilibrium. We showed that the condition of DNB in diffusive equilibrium is satisfied when the temperature in the burning layer  $T(\rho) < 4.55 \times 10^7 \rho_5^{-0.11} \text{ K}$  (CB03). The particular model that we have chosen ( $T_e = 1.5 \times 10^6 \text{ K}$ ) is in the diffusion limited regime and illustrates the reduction in the burning rate when diffusion becomes the rate limiting step. Compared to the calculation assuming diffusive equilibrium, incorporating diffusion effects decreases the burning rate,  $\zeta_H$ , by a factor of 25. This difference between a naive calculation which assumes diffusive equilibrium with one that includes the effects of diffusion gets even larger at high  $T_c$ 's.

The effect of incorporating the effects of diffusion into the DNB calculation is illustrated by Figure 2, which shows the H column lifetime,  $\tau_{\text{col}}$ , as a function of core temperature,  $T_c$ . In nuclear limited DNB, the column burning rate follows the scalings derived in CB03 for H/C,  $\tau_{\text{col}} \propto y_H^{-5/12} T_c^{-9.8}$  (for a range of  $T_c$  between  $2-4 \times 10^7 \text{ K}$ , but as noted in CB03, the scaling varies depending on the temperature we expand about; for lower temperatures,  $T_c < 2 \times 10^7 \text{ K}$ , the exponential scaling with

$T_c$  is -12 to -13). As we transition to diffusion limited DNB, the scaling with central core temperature becomes more gentle as shown in Figure 2. The scaling of  $\tau_{\text{col}}$  with total H column,  $y_H$ , remains the same as in nuclear limited DNB, since the H number density in the burning layer scales like  $\propto y_H^{-\delta_i}$  (CB03), where  $\delta_i = (Z_i + 1)/A_i - 2 \approx -1.42$  for H on C, and is totally independent of the details of the burning.

### 3. EFFECTS OF STRONG MAGNETIC FIELDS ON DNB

In order to apply our work to radio pulsars, we must include the effects of strong magnetic fields ( $B \sim 10^{12}$  G) on the micro-physics of the NS envelope. Magnetic fields of  $> 10^{11}$  G affect the thermal structure of the envelope by modifying the electron equation of state and opacity (for a review see Lai 2001 and references therein). The changes to the electron equation of state modify the electric field, which modifies the diffusion problem. However, we neglect magnetic effects on the ions since magnetic fields  $> 10^{16}$  G would be required to modify the ion EOS.

To model the full range of the electron EOS and opacity, we adopt the formalism of Potekhin & Yakovlev (2001) and references therein to relate the electron pressure and electron number density to the chemical potential. We calculate the chemical potential from the local pressure by modifying the iterative procedure described by Potekhin & Yakovlev (1996). The free-free opacity in a magnetic field is from equation (21) and (22) of Potekhin & Yakovlev (2001). For electron conduction opacities, we use the results of Potekhin (1999). Starting from the photosphere at  $\tau = 2/3$ , our numerical integration of the constant flux equation (9) for the magnetized envelope agree to within 1% with the thermal profiles (i.e.  $T(\rho)$ ) given by

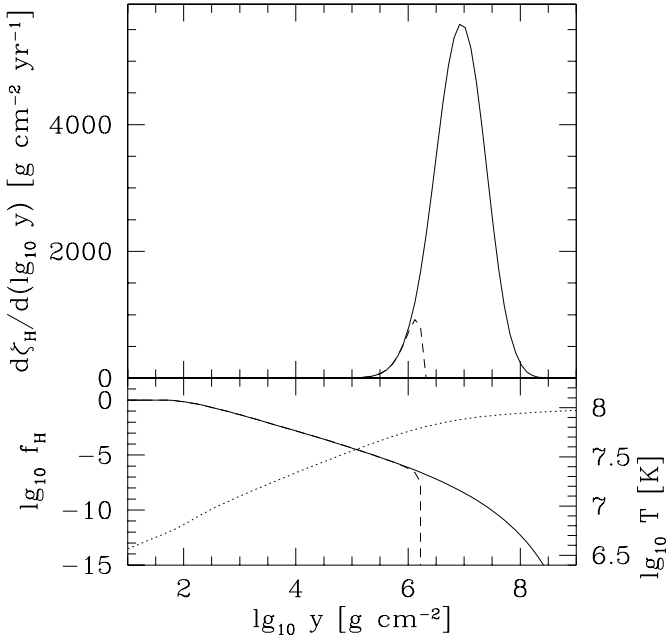


FIG. 1.— Total burning rate of H taking into account p-p capture and p +  $^{12}\text{C}$  capture. The bottom panel shows the number fraction,  $f_H = n_H/n_{\text{tot}}$ , and temperature (dotted line) as a function of column. This particular model has a total H column of  $100 \text{ g cm}^{-2}$  with an effective temperature of  $1.5 \times 10^6$  K. For the burning rate and number fraction, the dashed lines are the solutions taking diffusion limiting into account. The solid lines are the solutions assuming diffusive equilibrium (CB03). Assuming diffusive equilibrium, the burning rate of this model is  $\zeta_H \approx 6300 \text{ g cm}^{-2} \text{ yr}^{-1}$ . When diffusion limiting is taken into account, the burning rate is  $\zeta_H \approx 400 \text{ g cm}^{-2} \text{ yr}^{-1}$ .

Potekhin et. al. (2003) for accreted magnetized envelopes.

The thermal structure of a Hydrogen on Carbon magnetized envelope is given in Figure 3 for magnetic fields of various strengths and orientation, which we define in terms of  $\theta$ , the angle of the magnetic field relative to the radial direction. These NSs have surface gravities of  $g = 2.43 \times 10^{14} \text{ cm s}^{-2}$ , for a  $1.4 M_{\odot}$ , 10 km NS with an effective temperatures of  $T_e = 10^6$  K. We also show the nonmagnetic case (dotted line) for purposes of comparison. Compared to the nonmagnetic case, the magnetic envelopes are different in several respects. For a magnetic field with a significant radial component (i.e.  $\cos \theta = 1$  or 0.5), the base temperature is lower for a given effective temperature compared to the nonmagnetic case, while for more horizontally oriented magnetic fields, the base temperature is higher for a given effective temperature, highlighting the effect of magnetic field orientation on the opacity of the envelope. The transition from primarily radiative to primarily conductive heat transport, after which the envelope becomes isothermal, takes place at larger column and hence higher density compared to the nonmagnetic case. For the magnetic cases, orientation rather than field strength is a stronger determinant of the thermal profile, because the opacities along the field lines are a 4-7 orders of magnitude less than opacities across the field lines (for a review see Potekhin & Yakovlev 2001 and references therein). Therefore the temperature distribution is highly latitude dependent, with the star hotter at the magnetic poles and cooler at the magnetic equator.

The electric field determines the Hydrogen concentration,  $f_H$ , in the Carbon layer (CB03) and is a function of the adiabatic index,  $\chi_{\rho} = (d \ln P_e / d \ln \rho) \propto (d \ln P_e / d \ln n_e)$ . In the absence of magnetic effects, the adiabatic index undergoes a smooth transition from  $\chi_{\rho} = 1$  in the ideal gas case to  $\chi_{\rho} = 5/3$  in nonrelativistic degeneracy to  $\chi_{\rho} = 4/3$  in relativistic degeneracy. How-

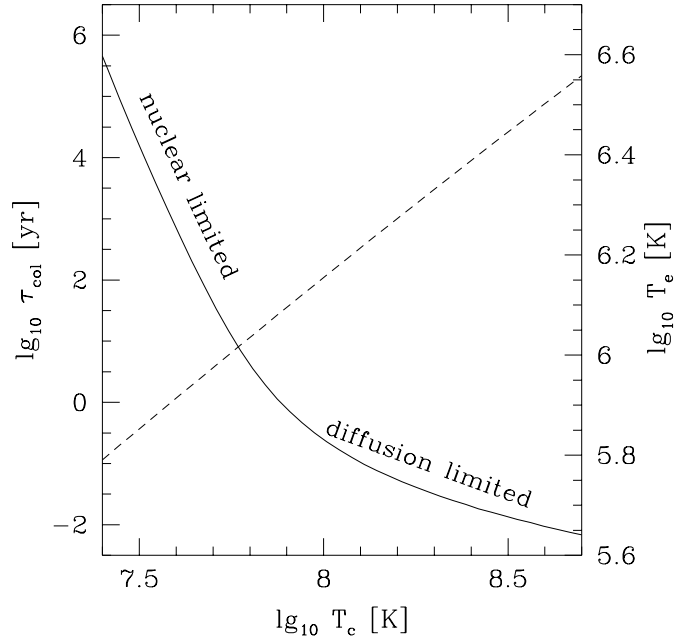


FIG. 2.— Lifetime (solid line) of Hydrogen with a fixed total column,  $y = 100 \text{ g cm}^{-2}$  on Carbon and effective temperature (dashed line) as a function of core temperature. The model with effective temperature,  $T_e = 10^6$  K, or core temperature,  $T_c = 5.5 \times 10^7$  K, represents the transition from the nuclear limited to diffusion limited regimes of DNB for H on C.

ever, in the presence of a quantizing magnetic field, the adiabatic index also undergoes de Haas-van Alphen oscillations in the weakly quantizing regime (Potekhin, Chabrier & Shibanov 1999b; Lai 2001) that also appears in the electric field.

Figure 4 shows the adiabatic index,  $\chi_\rho$ , and electric field as a function of density for the nonmagnetic case ( $B = 0$ ),  $B = 10^{12}$  G and  $B = 10^{13}$  G. The de Haas-van Alphen oscillations are evident as the electron EOS adiabatic index climbs from the value for the ideal gas equation of state to that of a 1-D Fermi gas,  $P_e \propto \rho^3$ . As the Fermi energy,  $E_F$  exceeds the integer values of the cyclotron energy, the equation of state softens, leading to alternating rising and falling of the adiabatic index and electric field. These oscillations are smeared out at the larger densities and temperatures deeper in the NS as  $E_F$  greatly exceeds the cyclotron energy and we recover the nonmagnetic solution.

For simplicity, we have ignore the effects of a strong magnetic field on diffusion. However, we expect the effects of magnetic fields on diffusion in the burning region is of little importance at typical pulsar fields. The following estimate illustrates this point. The mean free path for proton diffusion across magnetic fields is roughly given by the proton-gyro radius which is given by  $r_{g,p} = \sqrt{E/m_p}/\omega_B \approx 10^{-8}(T/10^8 \text{ K})^{1/2}B_{12}^{-1} \text{ cm}$ , where  $\omega_B = eB/(m_p c)$  is the cyclotron frequency. The mean free path for proton diffusion is given by the mean ion spacing  $a = [3\rho/(4\pi A m_p)]^{-1/3} \approx 4 \times 10^{-10} \rho_5^{-1/3} A^{1/3} \text{ cm}$ . Since the ion spacing is typically an order of magnitude smaller than the proton-gyro radius, we expect the effects of typical pulsar magnetic field on diffusion in the burning region to be small. Magnetic effects on diffusion is significant in the low density regions of the envelope ( $\rho \sim 10 \text{ g cm}^{-3}$ ), but changes to the diffusion coefficient in this region is of little importance to diffusion-limited DNB. For magnetar strengths, this is no longer the case and the effects of magnetic fields on diffusion must be taken into account.

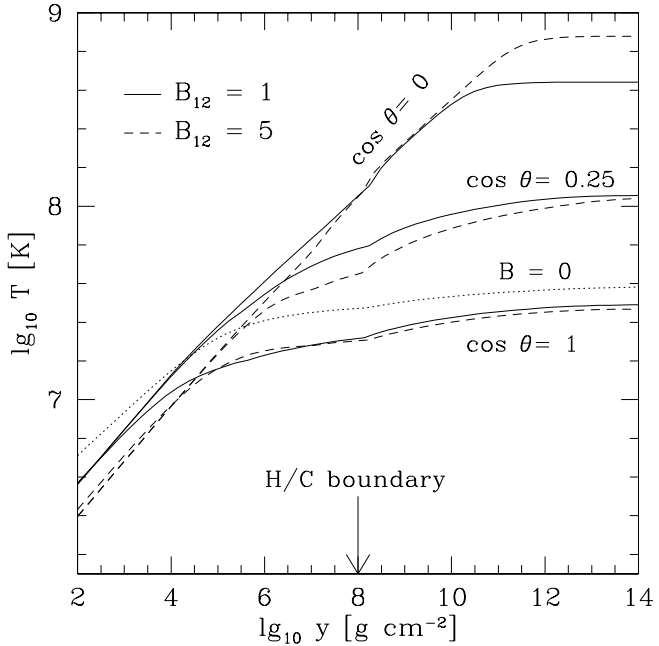


FIG. 3.— Thermal structure of a magnetic neutron star envelope for various values of field strength and inclination where  $\cos\theta = 1$  is the magnetic pole. The effective temperature is fixed at  $T_e = 10^6$  K and a H/C envelope is assumed with the H/C boundary at  $y = 10^8 \text{ g cm}^{-3}$ . The thermal structure for a B=0 envelope is shown by the dotted line.

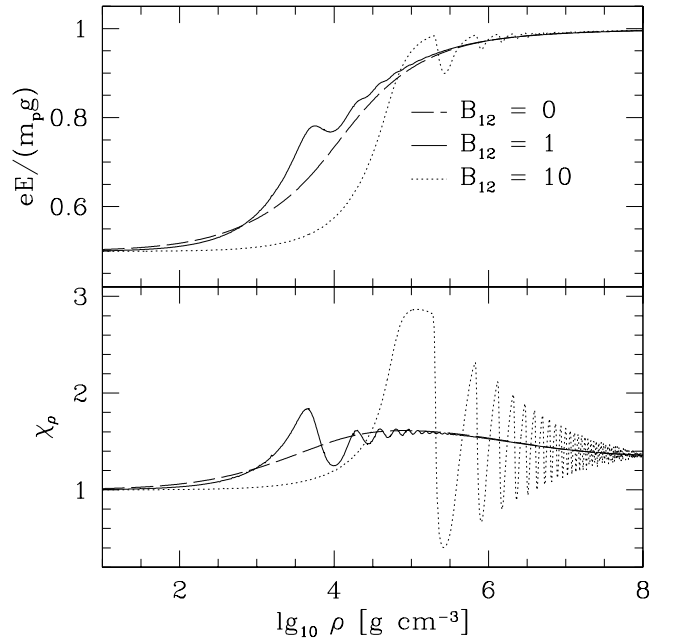


FIG. 4.— Electric field and adiabatic index  $\chi_\rho = d \ln P_e / d \ln \rho$  for a pure H envelope for various B-fields. The shift of the degeneracy point for the higher B-field case is readily apparent for the  $B = 10^{13}$  G case. The initial approach of the adiabatic index to three for the higher B-field case and the response of the de Haas-van Alphen oscillations to B-field strength is also shown. As expected all three cases asymptotically approach the relativistic degenerate limit of  $eE/m_p g = 1$  and  $d \ln P_e / d \ln \rho = 4/3$ .

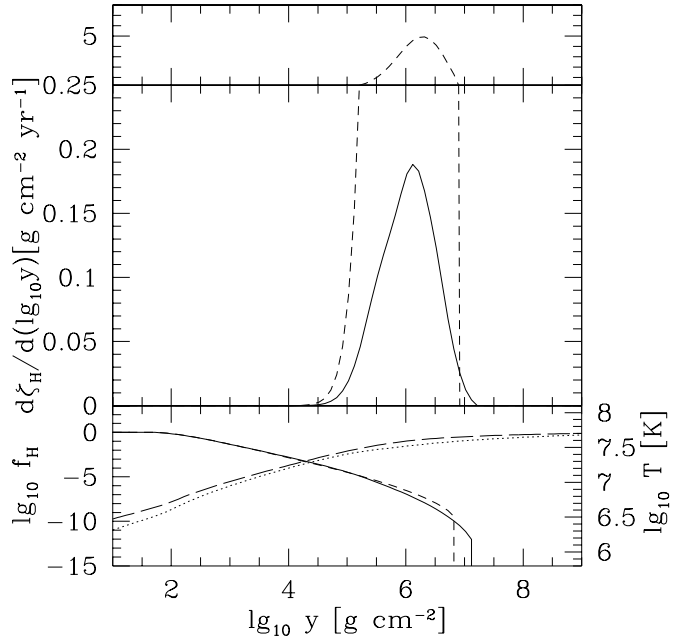


FIG. 5.— Total burning rate of H taking into account p-p capture and  $p + {}^{12}\text{C}$  capture for a magnetized envelope with  $B = 10^{12}$  G at the magnetic pole ( $\cos\theta = 1$ ) and unmagnetized envelope with the same core temperature,  $T_c = 5.5 \times 10^7$  K, and the same total H column,  $y_H = 100 \text{ g cm}^{-2}$ . The bottom graph shows the number fraction and temperature as a function of column for the magnetized (solid and dotted lines) and unmagnetized (dashed and long-dashed lines) envelopes. The nonmagnetic envelope has a column lifetime of  $\tau_H \approx 7 \text{ yr}$ , while the magnetic envelope has  $\tau_H \approx 200 \text{ yr}$  at  $B = 10^{12}$  G.

In Figure 5, we plot the burning integrand,  $d\zeta_H/(d\ln y)$ , for a model envelope with  $T_e = 1.125 \times 10^6$  K,  $B = 10^{12}$  G at the magnetic poles ( $\cos \theta = 1$ ) and compare this against unmagnetized model with the same core temperature and same total H column,  $y_H$ . Compared to the unmagnetized model, the magnetized model at  $B = 10^{12}$  G burns at a rate that is an order of magnitude less compared to the unmagnetized model. The reason for this lowered burning rate is a combination of lowered H number density and lowered temperature at the burning layer. The bottom plot of Figure 5 illustrates both points. At the burning layer (which is roughly the same for the magnetized and unmagnetized cases), the magnetized case for  $B = 10^{12}$  G has both lowered temperature and lowered H number density. Another crucial difference is that, despite possessing the same core temperature,  $T_c = 5.5 \times 10^7$  K, the magnetic envelope ( $B = 10^{12}$  G) has a higher effective temperature ( $T_e \approx 1.1 \times 10^6$  K) than the nonmagnetic case ( $T_e \approx 10^6$  K) due to the lower radiative opacity of highly magnetized plasmas.

Because the H number density or concentration and temperature profile are both modified by the presence of a quantizing B-field, the magnetic effects on DNB are nontrivial. The B-field always lowers the temperature at a *fixed column* for fixed  $T_c$  as shown in the bottom plot of Figure 5. The higher effective temperature of the magnetized envelope is wholly due to the increase in depth where the photosphere sits. If the burning layer was at a fixed column, this would suggest that increasing the B-field tends to decrease the DNB burning rate. In Figure 5, the difference in temperature at a given  $y$  between the magnetized envelope and  $B = 0$  envelope is about 12%, which gives a factor of five difference in the capture rates between the two. Also the transition region between the radiative outer envelope and isothermal inner envelope and core (the sensitivity strip) moves toward greater column or density with increasing B-field (Ventura & Potekhin 2001). This would also decrease the DNB burning rate as the burning layer moves to deeper depth and hence decreasing H number density (at least in the case of nuclear limited DNB). Also as illustrated in Figure 4, the electric field in the  $10^{12}$  G magnetized envelope is on average *higher* leading up to the burning region ( $\rho \sim 10^{4-5}$  g cm $^{-3}$ ) than in the nonmagnetized envelope. This results in a lower number density at a given column in the magnetized envelope ( $B = 10^{12}$  G) compared to the nonmagnetized envelope, as shown in the plot of number concentration as a function of column in Figure 5. Hence, we find for a  $B = 10^{12}$  G field, the DNB burning rate is reduced by a combination of a modified thermal profile and a modified electric field, but for stronger fields the situation may be significantly different and is a topic of further study.

We plot the H column lifetime as a function of the central core temperature for differing inclinations of a  $B = 10^{12}$  G with  $y_H = 100$  g cm $^{-2}$  in Figure 6. For purposes of comparison, we also show the nonmagnetic case (thick solid line). The low and high temperature scalings of the magnetized envelope are similar to the scalings the nonmagnetized envelope, but the overall normalization and transition temperature are modified by the magnetic field. *The H column lifetime is greater for the magnetized envelopes at  $B = 10^{12}$  G than for the unmagnetized envelopes for at a given  $y_H$  and  $T_c$ , but the magnitude of the change is highly dependent on the orientation of the magnetic field.* In the bottom plot, we show the effective temperature as a function of  $T_c$ . The variance in column lifetime and effective temperature are mainly due to the modification of the temperature profile by the magnetic field especially in the conductive

part of the envelope.

For a dipole geometry, Figure 7 shows the latitude dependence of the effective temperature and column lifetime for fixed  $T_c$ , dipole field strength ( $B_p = 10^{12}$  G) and total H column of  $y_H = 100$  g cm $^{-2}$ . The effective temperature and burning rate are greatest at the magnetic poles and smallest at the equator. At the magnetic equator the burning rate is reduced by about two orders of magnitude, while the effective temperature is reduced by about a factor of three. This change in effective temperature and column lifetime is mainly due to magnetic field inclination changing the region where the burning layer sits. From this plot, roughly 60% of the NS surface has the same burning rate (within 50%) and effective temperature (within 30%). Since H is preferentially depleted near the magnetic poles, this may induce a surface current of H from the equator to the poles, a problem that merits further study.

Much caution must be taken when looking at these results seriously especially in the superstrong B-field case since the effects of plasma non-ideality become more and more pronounced. Changes in the ion and electron equation of state due to Coulomb interactions changes the electric field in these envelopes, possibly altering the diffusion problem drastically.

#### 4. SURFACE COMPOSITION EVOLUTION FOR YOUNG RADIO PULSARS

The clear application of our theoretical work is to young radio pulsars, which can have both the nuclear physics of DNB active, but also, potentially mass loss via pulsars winds. Given the uncertainty in fallback models, the ease (in terms of availability) with which H can be accreted or produced by fallback (i.e. spallation; Bildsten et al. 1992), and the tiny amount of

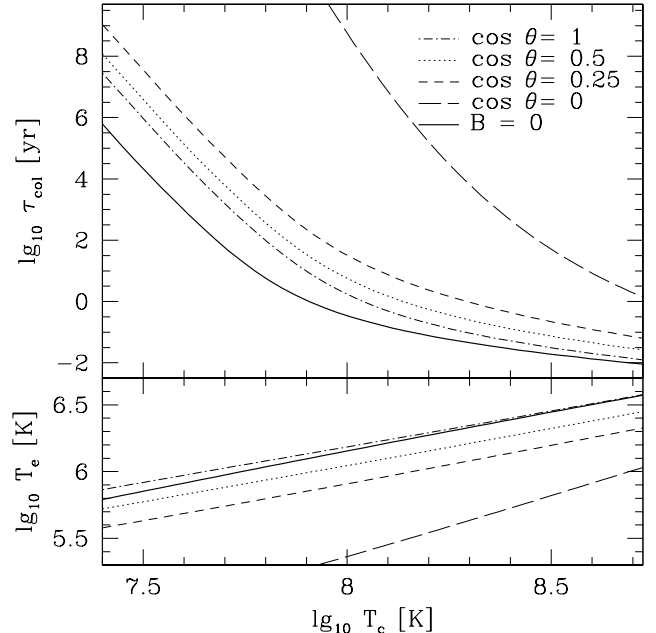


FIG. 6.— Hydrogen column lifetime and effective temperature for H on C envelopes as a function of core temperature  $T_c$  for different magnetic field inclinations, where  $\cos \theta = 1$  are the magnetic poles. The total H column is fixed at  $y_H = 100$  g cm $^{-2}$ . The magnetic field strength is  $B = 10^{12}$  G, typical of young radio pulsars. For a given core temperature the effective temperature of the magnetized object is greater for radial inclinations of the magnetic field, but the column lifetime of H is greater for the magnetized envelopes, regardless of inclination, than the nonmagnetic case (thick solid line).

material ( $\sim 10^{-19} M_{\odot}$ ) that comprises the NS photosphere, NS atmospheres should comprise mainly of Hydrogen. Furthermore, the strong gravity ( $g \sim 2-3 \times 10^{14} \text{ cm s}^{-2}$ ) on the surface of a NS implies that the sedimentation timescale is of order one second (Bildsten, Chang & Paerels 2003) and hence the photosphere should be pure H. Hence we would expect that all young NSs possess surface H at early times, but when the surface H begins to evolve depends on when the fallback episode ends, which is very uncertain.

#### 4.1. Surface Evolution via DNB

In Figure 8 we show the photospheric H lifetime ( $\tau_{\text{col}}$  at the photosphere) curves (i.e. implied  $T_c$  for a given lifetime) for  $B = 0$  and  $B = 10^{12} \text{ G}$  and proton capturing elements C and O. With the view that H could either be initially present or added at late times, we must compare these burning rates to the amount of time the NS spends with this  $T_c$ . These times are available from NS cooling calculations, and in Figure 8 we overlay a few representative cooling tracks (long-dashed lines). We include a standard cooling track which presumes modified URCA cooling on a  $1.3 M_{\odot}$  NS and another with core proton superfluidity (Potekhin et al. 2003). D. G. Yakovlev kindly calculated a model for us with triplet-state neutron superfluidity in the core with a critical temperature of  $8 \times 10^8 \text{ K}$ .

This figure makes clear that for H overlaying C, the burning time is always much less than the pulsar's age for the first  $10^{5-6}$  years. After this active DNB phase, any new H could stably exist on the photosphere. For H on O, we find that the active DNB phase depends more sensitively on the NS cooling and varies from  $10^{4-6}$  yrs. This implies that H deposited on the sur-

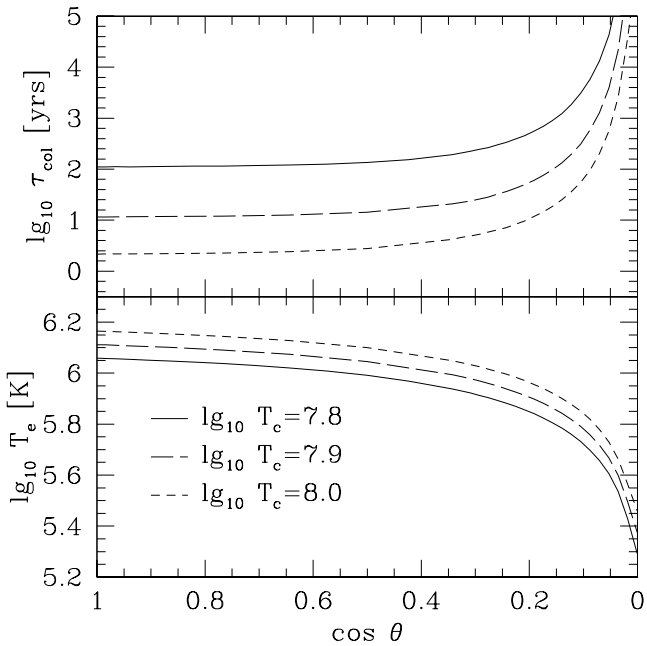


FIG. 7.— Hydrogen column lifetime for  $y_H = 100 \text{ g cm}^{-2}$  and effective temperature for H on C envelopes as a function of inclination to the magnetic pole  $\theta$ , presuming a dipole field configuration,  $B = B_p (\hat{r} \cos \theta + \hat{\theta} \sin \theta / 2)$ , where  $B_p = 10^{12} \text{ G}$ , for three different core temperatures,  $T_c = 6.3, 8, 10 \times 10^7 \text{ K}$ . The lifetime  $\tau_{\text{col}}$  changes by almost two orders of magnitude with latitude while the effective temperature changes only by a factor of a few. The variation in burning rate with latitude at fixed  $T_c$  is due to the changing temperature of the burning layer due to magnetic field inclination.

face of a rapidly cooling NS after  $10^5$  years could exist stably if the underlying material is Oxygen or heavier. No matter what, the active DNB phase does not naturally provide an explanation for the  $10^{4-5}$  yr timescale for surface evolution implied by the observations.

The recent observations of mid-Z atomic lines on 1E 1207.4-5209 implies that any surface Hydrogen must have been depleted on at least a  $10^4$  yrs timescale (Sanwal et al. 2002; Mereghetti et al. 2002; Hailey & Mori 2002; Mori & Hailey 2003). This pulsar is associated with the SNR, G296.5+10; the age by association is  $\approx 7$  kyr (Roger et al. 1988). The spectral features have been interpreted as either Oxygen lines ( $B_{12} = 0.55-0.75$ ,  $z = 0.06-0.21$ ) or Neon lines ( $B_{12} = 0.8-1.1$ ,  $z = 0.62-0.86$ ) (Mori & Hailey 2003). They have also been interpreted as He lines in a  $B \sim 10^{14} \text{ G}$  field, but this would require a special magnetic geometry in order to agree with the spindown B-field of  $B_{12} \approx 2-4$  (Pavlov et al. 2002b; Sanwal et al. 2002).<sup>1</sup>

Let us take the interpretation of these spectral features as Oxygen lines. Mori & Hailey's (2003) interpretation of the spectral features as Oxygen lines yielded  $B = 5.5-7.5 \times 10^{11} \text{ G}$  with a redshift of  $z = 0.06-0.21$ . Though it is not self-consistent, we use the  $T_e \approx 1.1 \times 10^6 \text{ K}$  from the H atmosphere fit of Mereghetti et al. (2002). For Mori & Hailey's combination of redshift and B-field, we find that the H lifetime at the photosphere varies from 2-20 kyr for an underlying Oxygen layer. Hence, it is plausible that DNB has occurred on the surface of this NS to deplete any surface H (*if initially present*) to reveal the under-

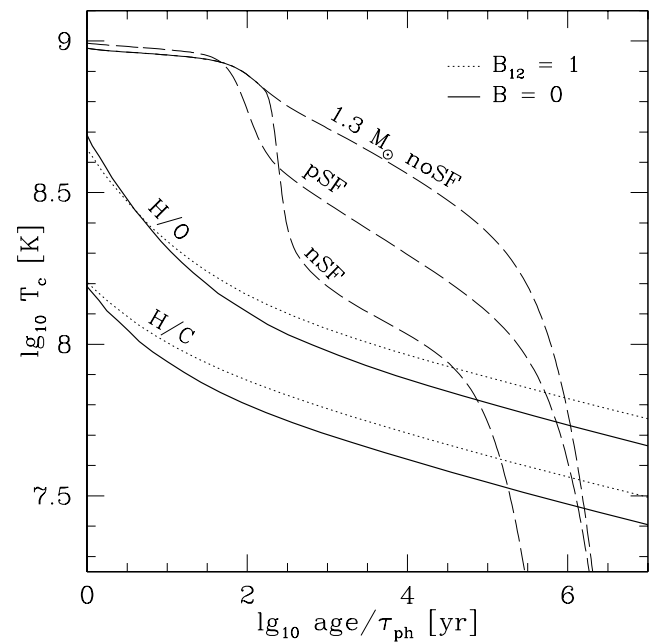


FIG. 8.— H column lifetime curves for H on C and H on O envelopes at the magnetic poles for different  $B_p = 0$  (thick solid line),  $10^{12} \text{ G}$  (dotted line). Overlayed are cooling tracks (long-dashed lines) for various NS models (Potekhin et al. 2003) including standard cooling (no superfluidity, modified Urca cooling represented by  $1.3 M_{\odot}$  nosSF), proton superfluidity (pSF) and triplet-state core neutron superfluidity (nSF) with critical temperature  $\approx 8 \times 10^8 \text{ K}$ .

<sup>1</sup> More recent observations indicate that there are additional lines at 2.1 and 2.8 keV (Bignami et al. 2003), which would render the interpretation of these lines as electron cyclotron lines, but these results require further study. The electron cyclotron lines would indicate a magnetic field strength of  $B = 6 \times 10^{10} (1+z) \text{ G}$ .

lying proton-capturing element, Oxygen.

#### 4.2. Surface Composition Evolution via Pulsar Wind Mass Loss

In addition to DNB, the surface evolution of magnetized rotating NSs may also be driven via outgoing pulsar winds. Though there is debate about whether nuclei are present in the pulsar wind (Goldreich & Julian 1969; i.e. see Ruderman and Sutherland 1975), it is still helpful to estimate how much material could possibly be excavated from an active pulsar's surface. Gallant and Arons (1994) analysis of the Crab pulsar winds showed that the ions leave that pulsar roughly at the rate of the Goldreich-Julian current flow from the polar cap region,

$$\dot{N}_i \approx \frac{2\Omega^2 \mu \cos i}{ec}, \quad (16)$$

where  $\mu$  is the NS magnetic moment. We integrate this over time to find the total number of excavated ions,  $N = \int N_i dt$  (Michel 1975). For a constant magnetic moment (i.e. no field decay), the time integral can be turned into an integral over the spin frequency using the magnetic dipole spin-down law,  $\dot{\Omega} = -2\mu^2\Omega^3 \sin^2 \theta / 3Ic^3$ , where  $I$  is the NS moment of inertia and  $\theta$  is the angle between the spin axis and magnetic moment. This gives Michel's (1975) estimate of the total number of ions,

$$N_{\text{exc}} \approx \frac{3Ic^2 \cos i}{\mu e \sin^2 \theta} \ln \left( \frac{\Omega_i}{\Omega_f} \right), \quad (17)$$

that have been excavated from the NS surface as it spins down from  $\Omega_i$  to  $\Omega_f$ .

Though this has never been shown, we will presume that the long excavation timescale (of order the spin-down time) allows the polar "hole" left by the exiting ions to be filled in by flow of material from other parts of the NS. Taking the moment of inertia as  $I \approx 0.4MR^2$  (Ravenhall and Pethick 1994), the excavated column depth (presuming pure Hydrogen) is

$$y_{\text{exc}} \equiv \frac{m_p N_i}{4\pi R^2} \approx \frac{M m_p c^2}{10\mu e} \ln \left( \frac{\Omega_i}{\Omega_f} \right), \quad (18)$$

where we dropped the angular factors. Putting in fiducial numbers, we find a total excavated column density

$$y_{\text{exc}} \approx 10^9 \text{ g cm}^{-2} \left( \frac{M}{1.4M_{\odot}} \right) \left( \frac{10^{30} \text{ G cm}^3}{\mu} \right) \ln \left( \frac{\Omega_i}{\Omega_f} \right), \quad (19)$$

which is comparable to the maximum amount of Hydrogen (Bildsten & Cumming 1998) or Helium (Cumming & Bildsten 2000) that can be present on young NSs with hot cores.

Though the physics of the pulsar wind is by no means well understood, excavation has testable observational consequences for magnetized spinning NSs. Since  $y_{\text{exc}}$  is very sensitive to the NS's magnetic dipole moment, the possible repercussions are diverse. For conventional radio pulsars, the underlying material may be unveiled during the initial cooling phase ( $< 10^6$  yrs). For magnetars and AXP's, a large layer of overlying material can survive on the NS. However, for millisecond radio pulsars, the amount excavated is so large that the rp-process ashes from the mixed Hydrogen-Helium burning during the accretion phase (see Strohmayer & Bildsten 2003 for an overview) might well be revealed.

## 5. CONCLUSIONS

Supernova theory cannot predict the surface composition of a young neutron star. The range of possible *initial* surface

compositions is large, depends on fall-back physics and residual burning at early times (i.e.  $< 1 - 10$  years). Hence, we focused here on tracing the abundance evolution for different initial states in the hopes of connecting them to possible final states. This has allowed us to construct a guide to the observer (Table 1) on the astrophysical implications of secure detections of specific elements. Before explaining this observational guide in detail, we summarize our main physics results.

We have extended our original study of DNB (CB03) to include burning when diffusion is the rate limiting step and the important effects of surface magnetic fields in the context of a highly approximate model of the envelope and diffusion physics. When diffusion is the rate limiting step, we modified the basic equations of the envelope by including an extra "diffusion" equation with an nuclear driven sink. By including magnetic effects, we can now apply our work to young radio pulsars. We have shown that H can be depleted in  $10^6$  years from the surface of a magnetized neutron star by diffusively burning in deeper C layers. The timescale of this burning depends primarily on three NS parameters: the core temperature, magnetic field and nuclear composition of the layers where the proton captures occur. For magnetic fields typical of young radio pulsars ( $B \sim 10^{12}$  G) with an underlying C layer, we have shown that the active DNB phase is relatively long (up to  $10^6$  yrs). The active DNB phase gets shorter for heavier proton capturing elements. We applied our work to the recent observations of magnetized Oxygen lines from 1E 1207.4-5209 and showed that (if initially present) Hydrogen would be depleted from the NS surface on a timescale comparable to its age ( $< 7$  kyr), exposing a pure Oxygen layer.

In section 4, we pointed out that the loss of ions in a pulsar wind may be a relevant mechanism for the surface evolution of magnetized, rotating NSs. Our estimate for the amount of material lost via the wind is comparable to the maximum amount of Hydrogen-Helium on the surface of the NS at birth. Though the mechanism for the wind is highly uncertain, this amount of excavated material may have significant observational consequences for young radio pulsars and MSPs.

There is one remaining complication that needs to be resolved, which is the impact of an intervening Helium layer on the H depletion rate. The He layer would need to displace the burning layer in order to significantly impact the rates. However, the degeneracy of such a thick He layer allows the He to readily diffuse downward into the underlying same A/Z matter. Hence, both Coulomb and thermal effects on the ion equation of state must be included to resolve the miscibility of the He with the underlying layers. This problem is also applicable to the study of stratification in cooling white dwarfs and will be addressed separately.

Given the sensitivity of DNB and excavation to the initial composition of the envelope and physics of the pulsar wind respectively, we can learn a tremendous amount from precision surface composition measurements of young  $B \sim 10^{12}$  G neutron stars. We have constructed a guide to understand such measurements in Table 1. Given the efficiency of DNB at the high  $T_c$  typical of young NSs, detection of H on a young pulsar would indicate that either continual accretion of H rich material is occurring, or a thick He buffer that blocks DNB is present, or there are no proton capturing elements present underneath the H. If H were detected on an older pulsar ( $> 10^6$  yrs), this would indicate that ion loss via pulsar wind excavation is minimal. Detection of He on a young radio pulsar ( $< 10^6$  yrs) would in-

dicate that the initial H was depleted (via either DNB or excavation) or that the material which fell back on the NS shortly after birth made no H. For NS older than  $10^6$  yrs (where here we presume this is roughly the pulsar spin-down time), detection of He would indicate that pulsar wind excavation is ineffective at removing He from the surface. Detection of CNO or heavier elements may indicate that the initial H/He (and CNO for heavy opaque material) pile was depleted via excavation (possibly DNB for H). Detection of CNO elements may also indicate that the outer shells had a “soft landing” fallback onto the NS after birth i.e. no spallation, if excavation is excluded. Finally, heavy opaque materials may also indicate lack of any fallback, if there is no excavation.

We thank A. Y. Potekhin for clarifying discussions on the nature of the electron EOS and opacities at high densities and

#### REFERENCES

Alcock, C. & Illarionov, A. 1980 ApJ, 235, 534  
 Baiko, D.A., Kaminker, A.D., Potekhin, A.Y. & Yakovlev, D.G. 1998, ApJ, 81, 25  
 Bignami, G. F., Caraveo, P. A., De Luca, A. & Mereghetti, S. 2003, Nature, 423, 725  
 Bildsten, L., Chang, P. & Paerels, F. 2003, ApJ, 591, L29  
 Bildsten, L. & Cumming, A. 1998, ApJ, 506, 842  
 Bildsten, L. & Hall, D. M. 2001, ApJ, 549, L219  
 Bildsten, L., Salpeter, E. E. & Wasserman, I. 1992, ApJ, 384, 143  
 Brown, E.F., Bildsten, L. & Chang, P. 2002, ApJ, 574, 920  
 Chang, P. & Bildsten, L. 2003, ApJ, 585, 464 (CB03)  
 Chabrier, G. & Potekhin, A. Y. 1998, Phys. Rev. E, 51, 4941  
 Chapman, S. & Cowling, T. G. 1952, *The Mathematical Theory of Non-Uniform Gases* (Cambridge: Cambridge University Press)  
 Chiu, H. Y. & Salpeter, E. E. 1964, Phys. Rev. Lett., 12, 413  
 Clayton, D. 1983, *Introduction to Stellar Structure and Nucleosynthesis* (Chicago: University of Chicago Press)  
 Cumming, A. & Bildsten, L. 2000, ApJ, 544, 453  
 Gallant, Y. A. & Arons, J. 1994, ApJ, 435, 230  
 Goldreich, P. & Julian, W. H. 1969, ApJ, 157, 869  
 Hailey, C. J. & Mori, K. 2002, ApJ, 578, L133  
 Hansen, J. P., McDonald, I. R., Pollock, E. L. 1975, Phys. Rev. A, 11, 1025  
 Kaminker, A. D., Yakovlev, D. G. & Gnedin, O. Y. 2002, A&A, 383, 1076  
 Lai, D. 2001, Rev. Mod. Phys., 73, 629  
 Michel, F. C. 1975, ApJ, 198, 683  
 Mereghetti, S., De Luca, A., Caraveo, P. A., Becker, W., Mignani, R. & Bignami, G. F. 2002, ApJ, 581, 1280  
 Mori, K. & Hailey C. J. 2003, submitted to ApJ, astro-ph/0301161  
 Paczynski, B. 1983, ApJ, 267, 315  
 Paquette, C., Pelletier, C., Fontaine, G., Michaud, G. 1986, ApJS, 61, 177  
 Pavlov, G. G., Zavlin, V. E. & Sanwal, D. 2002a, in Proceedings of the 270. Heraeus Seminar on Neutron Stars, Pulsars and Supernova Remnants, Bad Honnef (Germany), Jan. 21-25, eds. W. Becker, H. Lesch and J. Trümper  
 Pavlov, G. G., Zavlin, V. E., Sanwal, D. & Trümper, J. 2002b, ApJ, 569, L95  
 Potekhin, A. Y. 1999, A&A, 351, 787  
 Potekhin, A. Y., Baiko, D. A., Haensel, P. & Yakovlev, D. G. 1999a, A&A, 346, 345  
 Potekhin, A. Y., Chabrier, G. & Shibanov, Y. A. 1999b, Phys. Rev. E, 60, 2193  
 Potekhin, A. Y. & Yakovlev, D. G. 1996, A&A, 314, 341  
 Potekhin, A. Y. & Yakovlev, D. G. 2001, A&A, 374, 213  
 Potekhin, A. Y. & Yakovlev, D. G., Chabrier, G., Gnedin, O. Y. 2003, ApJ, 594, 404  
 Ravenhall, D. G., & Pethick, C. J. 1994, ApJ, 424, 846  
 Roger, R. S., Milne, D. K., Kesteven, M. J., Wellington, K. J. & Haynes, R. F. 1988, ApJ, 332, 940  
 Rosen, L. C., 1968, Ap&SS, 1, 372  
 Ruderman, M. A., & Sutherland, P. G. 1975, ApJ, 196, 51  
 Sanwal, D., Pavlov, G. G., Zavlin, V. E. & Teter, M. A. 2002, ApJ, 571, L61  
 Schatz, H., Bildsten, L., Cumming, A., & Wiescher, M. 1999, ApJ, 524, 1014  
 Strohmayer, T. & Bildsten, L. 2003 To appear in *Compact Stellar X-Ray Sources*, ed. W.H.G. Lewin and M. van der Klis (Cambridge University Press), astro-ph/0301544  
 Ventura, J. & Potekhin, A. Y. 2001, in *The Neutron Star–Black Hole Connection*, ed. C. Kouveliotou, J. Ventura, & E. van den Heuvel, Vol. 567, NATO ASI sec. C (Dordrecht: Kluwer), 393  
 Woosley, S. E. & Weaver, T. A. 1995, ApJS, 101, 181  
 Yakovlev, D.G., Kaminker, A.D., & Gnedin, O.Y. 2001, A&A, 379, 5

for generous and patient support throughout this work, D. G. Yakovlev for providing us with NS cooling models, and K. Mori for providing us with atomic line energies at large B-fields. We thank the anonymous referee for making very useful comments and suggestions. We would also like to thank P. Arras and C. J. DeLooye for valuable discussions on the nature of two-component plasmas at high densities and J. Heyl for some very helpful suggestions and discussions. We would also like to thank S. W. Davis, A. Socrates, and D. Townsley for discussions. P.C. would like to thank the Department of Physics and Department of Astronomy at Columbia University for their hospitality. This work was supported by the National Science Foundation under grants PHY99-07949 and AST02-05956, NASA through grant NAG 5-8658. L. B. is a Cottrell Scholar of the Research Corporation.

TABLE 1  
IMPLICATIONS OF OBSERVED SURFACE COMPOSITIONS OF YOUNG  $10^{12}$  G NEUTRON STARS

Measured Surface Composition		Age of NS	Astrophysical Implications	
H	$< 10^6$ yrs	continual accretion		
		- or - thick He buffer - or - no underlying p-capturing material		
He	$> 10^6$ yrs	same as for $< 10^6$ yrs		
		- and possibly - no excavation from pulsar wind		
C, N, O	$< 10^6$ yrs	initial H depleted via DNB/excavation		
		- or - spallation of fallback material without H production		
Heavy opaque elements	$> 10^6$ yrs	same as for $< 10^6$ yrs		
		- and possibly - no He excavation from pulsar wind		
		initial H/He depleted via DNB/excavation		
		- or - “soft landing” of outer shell material (no spallation)		
		excavation of initial H/He/CNO pile		
		- or -		
		no SN fallback ( $M_{\text{fallback}} < 10^{-19} M_{\odot}$ )		